

OPEN ACCESS

EDITED BY
Susanne M. Stieger-Vanegas,
Oregon State University, United States

REVIEWED BY
Lauren B. Priddy,
Mississippi State University, United States
Xiangwen Shi,
Kunming Medical University, China

*CORRESPONDENCE

Desheng Li

☑ lidesheng_ccrcgp@163.com

RECEIVED 11 February 2025 ACCEPTED 16 September 2025 PUBLISHED 09 October 2025

CITATION

Wang C, Yang H, Wu K, Deng L, Li C, Wei R, Li C, Zhu Y, Wei M, Huang Z, Cheng Y, Chen X and Li D (2025) Case Report: Osteomyelitis in a giant panda (*Ailuropoda melanoleuca*). *Front. Vet. Sci.* 12:1574668. doi: 10.3389/fvets.2025.1574668

COPYRIGHT

© 2025 Wang, Yang, Wu, Deng, Li, Wei, Li, Zhu, Wei, Huang, Cheng, Chen and Li. This is an open-access article distributed under the terms of the Creative Commons Attribution License (CC BY). The use, distribution or reproduction in other forums is permitted, provided the original author(s) and the copyright owner(s) are credited and that the original publication in this journal is cited, in accordance with accepted academic practice. No use, distribution or reproduction is permitted which does not comply with these terms.

Case Report: Osteomyelitis in a giant panda (*Ailuropoda melanoleuca*)

Chengdong Wang, Haidi Yang, Kai Wu, Linhua Deng, Chengyao Li, Rongping Wei, Caiwu Li, Yan Zhu, Ming Wei, Zhi Huang, Yanxi Cheng, Xuemei Chen and Desheng Li*

China Conservation and Research Center for the Giant Panda, Key Laboratory of SFGA on the Giant Panda, Chengdu, Sichuan, China

Osteomyelitis is an inflammatory disease of bone tissue induced by microbial infection, and poses a significant health burden in humans and animals. The global annual incidence in humans is estimated $\sim 1-10$ cases per 100,000 individuals, with notably higher rates observed in high-risk populations. In domestic cubs and companion animals, trauma-related osteomyelitis can occur at an incidence rate ranging from 0.1 to 5%. Although osteomyelitis is welldocumented in both human and veterinary medicine, with diverse and complex diagnostic and therapeutic approaches available for human cases, it has not been previously reported in the giant panda (Ailuropoda melanoleuca). This report presents a case of osteomyelitis in an elderly giant panda exhibiting lameness in the left hind limb. Diagnosis was confirmed trough laboratory testing, computed tomography (CT), and magnetic resonance imaging (MRI). The animal underwent a 2-month course of treatment with rifampicin (Guangzhou Baiyunshan Pharmaceutical Group Co., LTD) and medical-grade chitosan (Qingdao Jintieshan Biotechnology Co., LTD), which resulted in significant clinical improvement. This retrospective case analysis provides valuable insights into the clinical diagnosis and management of osteomyelitis in giant pandas and contributes to the foundational knowledge necessary for the prevention and treatment of this condition in captive populations.

KEYWORDS

giant panda (Ailuropoda melanoleuca), osteomyelitis, MRI, rifampicin, chitosan

1 Introduction

The giant panda (*Ailuropoda melanoleuca*), as a flagship species for global biodiversity conservation, requires meticulous health management, which is essential for the survival of this endangered species.

Osteomyelitis, a prevalent disease affecting both humans and vertebrates, poses significant threats to their health (1). It refers to an inflammation of the bone tissue, usually caused by bacterial infections, though fungal or viral pathogens can also be responsible (2, 3). Epidemiology shows humans like infants, the elderly and those with compromised immune systems are more susceptible (4). This disease is not exclusive to humans. In other animals, for example, dogs often suffer from osteomyelitis due to open fractures, bites from other animals, or spread of infections from other parts of the body (5, 6). Cats can also be affected, with juvenile cats being more prone to acute forms (7), while older cats may develop chronic osteomyelitis. In livestock such as cattle and sheep, osteomyelitis can occur as a result of injuries during grazing or fighting, and it may lead to significant

economic losses in the farming industry (8, 9). In the context of wildlife conservation, understanding osteomyelitis is crucial for the health management of endangered species like the giant panda. The symptoms and signs of osteomyelitis patients typically include swelling, warmth, redness at the infected site, pain, and mobility difficulties (10). However, a significant diagnostic challenge lies in the fact that sometimes osteomyelitis may present with no obvious signs or symptoms, or the symptoms are easily confused with other diseases (11). As for giant pandas, due to the unique characteristics of the species-their thick fur can mask localized swelling or redness and their pain can be masked and they may hide signs of pain-accurately identifying these symptoms can be even more difficult.

Laboratory tests play a role in diagnosing osteomyelitis. The majority of osteomyelitis cases are bacterial in origin, and laboratory findings often reveal elevated erythrocyte sedimentation rate (ESR) and C-reactive protein (CRP) levels (12). Relying solely on blood markers may lead to misdiagnosis as they can be elevated in various inflammatory conditions. Furthermore, conventional imaging modalities such as radiography (X-ray), computed tomography (CT), and magnetic resonance imaging (MRI), are also used in clinical assessment. Nevertheless, accurate diagnose across different stages of osteomyelitis remains a clinical challenge (13). Bone destruction usually needs to reach 30%-50% to be detected on X-rays, so X-rays may not detect earlystage osteomyelitis, because soft tissue swelling and reduced mineral opacity may be subtle and can be overlooked during this period (14, 15). Computed tomography (CT) is an advanced imaging technique based on X-ray technology that provides highresolution cross-sectional images of internal anatomical structures. A key advantage of CT is its rapid imaging acquisition enabling comprehensive scans to be completed in a short time, which is an essential feature for prompt diagnosis in a critical care setting (16, 17). In veterinary medicine, this rapidity is particularly valuable given the challenges of anesthetizing non-human species—wild animals often tolerate anesthesia poorly (18), and CT's short scan times reduce risk of anesthesia related complications. While CT provides excellent visualization of subchondral bone and cortical bone, its ability to assess tendinous and ligamentous soft tissues is limited, particularly without contrast enhancement (19, 20). Equine studies have demonstrated that contrast-enhanced CT improves the evaluation of tendons and ligaments. In addition, CT can depict early inflammatory changes, such as loss of fat planes and soft tissue swelling. Therefore, CT should be considered to complementary to other imaging modalities rather than a standalone technique for soft tissue assessment. In the early stages of osteomyelitis, CT may fail to demonstrate subtle findings such as early bone marrow edema or the slightest periosteal reaction (21). MRI, which uses magnetic fields and radio frequency pulses, provides excellent soft tissue contrast (22). When used in combination, MRI and CT enhance diagnostic accuracy by providing complementary information: CT excels in delineating bony architecture, whereas MRI is highly sensitive to marrow edema and soft tissue inflammation. Both modalities are widely applied in the clinical diagnosis of osteomyelitis and are welldocumented in the literature (23–25).

This report for the first time details the diagnosis and symptomatic treatment of osteomyelitis in an elderly giant panda with lameness through hematology, biochemistry, computed tomography (CT), and MRI.

2 Case presentation

A male giant panda, \sim 26 years old and weighing around 120 kg, was previously healthy with no significant medical history. This animal developed acute lameness, which significantly restricted mobility. Subsequently, within and a few days, the giant panda was unable to completely bear weight on the left hind limb (Figure 1a). In response to these concerning symptoms, the veterinary team decided to initiate a comprehensive clinical examination.

Initial clinical evaluation involved observation and palpation of the limbs, followed by blood collection for routine hematological and biochemical testing. A non-anesthetic examination revealed mild atrophy of the left hind limb, with no pain response on palpation. There was mild alopecia on the medial aspect of the left hind limb's thigh and increased skin temperature, without detected swelling, trauma, or joint deformity. Additionally, claw abrasion was noted on the right paw, accompanied by erythema and swelling of the right paw pad (Figure 1b). No other abnormalities were detected during this initial assessment. Blood samples were collected concurrently for routine blood and biochemical tests, which subsequently revealed low lymphocyte and platelet counts, and the levels of total cholesterol (TC) and triglycerides (TG) were elevated. However, no significant increase in C-reactive protein (CRP) was observed (since there was no reference range for CRP in giant pandas, human levels were used here; Table 1). Throughout this examination phase, the panda's diet and weight remained stable, consistent with its baseline status. 3 days later, under general anesthesia, further examination was performed. The panda's body temperature was normal, and no external injuries, or draining fistulas were observed. Subsequently, advanced imaging modalities were employed. Non-enhanced scanning of both hind limbs was performed using a Toshiba Activion 16 multislice CT scanner (TOSHIBA, Tokyo, Japan). The panda was placed in a dorsal recumbency. The scanning protocol included both hindlimbs, extending from the femur to the phalanges. A helical scan mode was used with a gantry rotation time of 0.5 s per rotation and a detector configuration of 16 rows × 1.0 mm. The beam collimation width was matched to the detector configuration $(16 \times 1.0 \,\mathrm{mm})$, with an original slice thickness of 1.0 mm. Tube voltage was set at 120 kV and tube current at 70 mA. The pitch was 1.375:1. The scan field of view (SFOV) was adjusted according to the number of hind limbs: 450 mm for bilateral and 400 mm for unilateral examinations. The Z-axis scanning range was ~600 mm, and the original slice thickness was fixed at 1.0 mm. Image reconstruction parameters were tailored to diagnostic needs. For bone evaluation, images were reconstructed with a slice thickness of 5.0 mm. For soft tissue evaluation, images were reconstructed with a slice thickness of 1.1 mm and a reconstruction interval of 0.69 mm. A high-resolution bone algorithm (Bone 5.0) was applied for bone reconstruction, and a standard soft tissue algorithm (Soft Tissue 1.1) was applied for soft tissue reconstruction. The reconstruction matrix was uniformly 512×512, with a pixel size of 0.8 mm. The display field of view

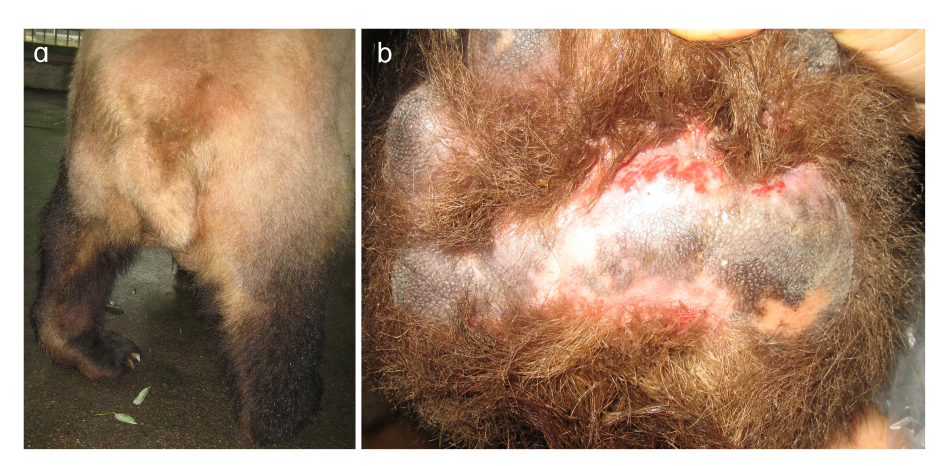


FIGURE 1

Clinical manifestations of the left hind limb in the affected giant panda. (a) Left hind limb of the giant panda. During ambulation, the plantar surface fails to make contact with the ground, resulting in severe locomotor dysfunction. (b) Abraded left hind paw pad of the giant panda. Prolonged abnormal weight-bearing avoidance led to redness and swelling.

(DFOV) was set to 350 mm. For the bone window, window width and level were 2,000 HU and 500 HU, respectively; for the soft tissue window, window width and level were 1,876 HU was 492 HU, respectively. CT scans revealed no evidence of fractures, joint space narrowing or widening, osteophyte formation, or other bony abnormalities in either hind limb (Figure 2). With the permission of the government, these CT scans were read jointly by radiologists and veterinarians, who confirmed that there were no osseous abnormalities in the two hind limbs. Following the CT examination, a Toshiba Vantage Titan 1.5T MRI (TOSHIBA, Tokyo, Japan) was used to perform MRI examinations. Image acquisition is carried out with a slice thickness of 3-5 mm and an interval of 1-2 mm. First, conventional SE sequences were used for image acquisition (T1W: TR 1,700 ms, TE 15 ms); T2W: TR 4,294 ms, TE 105 ms). T1W sagittal images of the tarsus show that the bony structures, including the distal tibia, talus, and calcaneus, have distinct and well-defined margins. The bone marrow signal within these bones is homogeneous, with no apparent abnormal hypointense or hyperintense areas detected. The articular cartilage of the tarsus maintains a smooth surface, and its signal intensity on T1W imaging is consistent with that of normal articular cartilage, appearing isointense relative to the adjacent muscle tissue in most regions. The tarsus ligaments, such as the dorsal talofibular ligament and calcaneofibular ligament (visualized in appropriate sections), exhibit normal low-signal characteristics on T1W sequences, without evidence of discontinuity, thickening, or abnormal signal intensity. The surrounding soft tissues, including the tendons (e.g., the Achilles tendon, tibialis cranial) and the joint capsule, display a normal layered structure, with no significant swelling, thickening, or abnormal signal intensity changes. The T2W transverse image shows that patchy high signals are found in the soft tissues around the distal tibia and the plantar aspect of the tarsus calcaneus, with indistinct edges. The signal intensity is higher than that of the adjacent normal muscle tissue. The high intensity around the distal tibia is mainly located in the interosseous space or interosseous muscle on the inner side of the distal tibia. The high signal plantar calcaneus is mainly distributed around the subcutaneous soft tissue on the inner, outer and plantar sides of the Achilles tendon (Figure 3). At the same time, there are also some high signal intensities in soft tissues of the plantar aspect of tarsus. Based on MRI findings, a diagnosis of osteomyelitis in the left hindlimb was made.

On the second day after the diagnosis, treatment was initiated. The giant panda was administered three cefixime capsules (100 mg per capsule, Guangzhou Baiyunshan Pharmaceutical Group Co., LTD, 2.5 mg/kg) twice daily. After 1 week of continuous administration, noticeable improvement was observed in the left hind limb. The pandas could exhibit normal plantigrade stance with the entire plantar surface of the hindlimbs touching the ground, and their overall activity level also increased. This situation persisted for 4 weeks without any further significant improvement. In response to this, the veterinarian adjusted the treatment plan, continuing the administration of three cefixime capsules (p.o., 2.5 mg/kg) twice daily and adding daily hind limb massages for 1 week. 3 days after this adjustment, the panda's condition improved, with a gradual increase in activity. Although the tiptoed gait persisted, the panda was able to support its body weight with both hind limbs. Given the instability of the condition, the medication was changed to rifampicin and chitosan 1 week later. Rifampicin (150 mg per capsule, Guangzhou Baiyunshan Pharmaceutical Group Co., LTD) and chitosan (200 mg per capsule, Qingdao Jintieshan Biotechnology Co., LTD) were administered orally, with five capsules of each taken on an empty stomach in the morning, and an additional five chitosan capsules (200 mg per capsule) given in the afternoon.

After 2 months of continuous treatment with the adjusted medication regimen, the symptoms were substantially relieved, and the medication was discontinued. 1-week post-discontinuation, no lameness and swelling were observed in the hind limbs. Moreover, the panda's overall demeanor, spirit, and appetite remained consistently good, and its fasting weight was maintained at 119 kg, indicating a successful resolution of the osteomyelitis episode and a return to a stable health status. During the subsequent

TABLE 1 Routine blood and biochemical test report of giant panda.

Terms	Code name	Results	Reference range	Evaluation
White blood cell count	WBC	6.0	$7.88 \pm 1.34 \times 10^9$ /L (39)	-
Lymphocyte count	LY#	1.8	$1.08 \pm 0.34 \times 10^9$ /L (40)	↑
Monocyte count	MONO#	0	$1.43 \pm 0.85 \times 10^9$ /L (41)	↓
Neutrophil count	NEUT#	4.2	$4.85 \pm 1.17 \times 10^9$ /L (39)	-
Lymphocyte ratio	LY%	30	27.02 ± 3.81% (39)	-
Monocyte ratio	MONO%	0	4.59 ± 1.15% (39)	↓
Neutrophil ratio	NEUT%	70	68.80 ± 3.37% (39)	-
Hemoglobin	HGB	104	119.98 ± 6.36 g/L (39)	↓
Red blood cell	RBC	6.39	6.12 ± 0.31 /L (39)	-
Hematocrit	HCT	32	33.32 ± 1.76% (39)	-
Mean corpuscular volume	MCV	50.1	54.78 ± 1.37 Fl (39)	↓
Mean corpuscular hemoglobin	MCH	20.9	19.62 ± 0.41 PG (39)	-
Mean corpuscular hemoglobin concentration	MCHC	418	358.48 ± 4.63 g/L (39)	↑
Coefficient variation of red blood cell volume distribution width	RDW-CV	14.8	16.33 ± 0.90% (39)	-
Standard deviation of red blood cell volume distribution width	RDW-SD	25.9	33.20 ± 1.53% (39)	+
Platelet count/blood platelet count	PLT	270	$525.77 \pm 96.45 \times 10^9$ /L (39)	\
Mean platelet volume	MPV	5.1	$6.05 \pm 1.04 \text{ Fl (40)}$	-
Platelet distribution width	PDW	15.3	9.93 ± 4.64 Fl (42)	↑
Thrombocytocrit	PCT	0.137	$0.31 \pm 0.05\%$ (39)	\
Potassium	Ka	5.6	4.83 ± 0.43 mmol/L (39)	-
Sodium	Na	125.3	129.09 ± 1.36 mmol/L (39)	-
Chlorine	Cl	97.7	97.44 ± 2.68 mmol/L (39)	-
Calcium	Ca	2.1	2.07 ± 0.11 mmol/L (39)	-
Phosphorus	P	0.12	$1.32 \pm 0.12 \text{ mmol/L (39)}$	\downarrow
Magnesium	Mg	0.79	0.99 ± 0.11 mmol/L (39)	-
Iron	Fe	20.3	30.80 ± 4.24 mmol/L (39)	\downarrow
Carbon dioxide combining power	CO ₂ -CP	21.0	22.32 ± 1.78 mmol/L (39)	-
Blood urea nitrogen	BUN	4.1	7.08 ± 1.15 mmol/L (39)	↓
Creatinine	Cr	85.3	101.90 ± 26.34 mmol/L (39)	-
Blood urea nitrogen/creatinine	BUN/Cr	0.05	0.09 ± 0.04 (39)	-
Uric acid	UA	20.3	56.68 ± 14.62 mmol/L (39)	\downarrow
Glucose	GLU	3.4	3.22 ± 0.40 mmol/L (39)	-
Osmotic pressure	OP	265.2	260-320 OSM (homo)	-
Triglyceride	TG	2.2	1.33 ± 0.31 mmol/L (39)	↑
Total cholesterol	TC	5.7	4.88 ± 1.15 mmol/L (39)	1
High density lipoprotein	HDL	4.2	$2.96 \pm 0.47 \text{ mmol/L (40)}$	1
Low-density lipoprotein	LDL	0.46	$3.41 \pm 1.46 \mathrm{mmol/L} (40)$	↑
Apolipoprotein A	ApoA	0.183	$0.71 \pm 0.18 \text{ g/L (40)}$	↓
Apolipoprotein B	АроВ	0.005	$0.04 \pm 0.03 \text{ g/L (40)}$	↓
Total protein	TP	74.9	65.83 ± 3.07 g/L (39)	↑
Albumin	ALB	30.3	34.31 ± 2.38 g/L (39)	\downarrow

(Continued)

TABLE 1 (Continued)

Total bile acids TBA 72.3 75.35 ± 10.18 μmol/L (42) - Alpha-hydroxybutyrate dehydrogenase α-HBDH 833.6 548.30 ± 297.50 U/L (39) - Lactate dehydrogenase LDH 951.8 632.59 ± 329.83 U/L (39) - Creatine phosphokinase CPK 175.8 194.96 ± 45.77 U/L (39) - Creatine kinase isoenzyme CPKIso 290.4 260.83 ± 67.56 U/L (39) - Myoglobin Mb 23.0 0-100 μg/L (homo) - Cholinesterase CHE 694.8 766.25 ± 232.49 (42) - Alkaline phosphatase	Terms	Code name	Results	Reference range	Evaluation
Alanine transaminase ALT 42.0 81.76 ± 19.84 U/L (40) ↓ Aspartate aminotransferase AST 67.3 71.93 ± 13.34 U/L (40) − Aspartate aminotransferase/alanine transaminase AST/ALT 1.6 0.91 ± 0.18 (40) ↑ Total bilirubin T-BIL 3.5 1.06 ± 0.29 μmol/L (39) ↑ Direct bilirubin D-BIL 1.2 0.51 ± 0.18 μmol/L (39) ↑ Indirect bilirubin I-BIL 2.3 0.55 ± 0.22 μmol/L (39) ↑ Total bile acids TBA 72.3 75.35 ± 10.18 μmol/L (42) − Alpha-hydroxybutyrate dehydrogenase α-HBDH 833.6 548.30 ± 297.50 U/L (39) − Lactate dehydrogenase LDH 951.8 632.59 ± 329.83 U/L (39) − Creatine kinase isoenzyme CPK 175.8 194.96 ± 45.77 U/L (39) − Creatine kinase isoenzyme CPKIso 290.4 260.83 ± 67.56 U/L (39) − Myoglobin Mb 23.0 0 −100 μg/L (homo) − Challine phosphatase ALP 116.	Globulin	GLB	44.6	$31.52 \pm 3.79 \text{ g/L } (39)$	↑
Aspartate aminotransferase AST 67.3 71.93 ± 13.34 U/L (40) − Aspartate aminotransferase/alanine transaminase AST/ALT 1.6 0.91 ± 0.18 (40) ↑ Total bilirubin T-BIL 3.5 1.06 ± 0.29 μmol/L (59) ↑ Direct bilirubin I-BIL 2.3 0.55 ± 0.22 μmol/L (59) ↑ Total bile acids TBA 72.3 75.35 ± 10.18 μmol/L (42) − Alpha-hydroxybutyrate dehydrogenase α-HBDH 833.6 548.30 ± 297.50 U/L (39) − Lactate dehydrogenase LDH 951.8 632.59 ± 329.83 U/L (39) − Creatine kinase isoenzyme CPK 175.8 194.96 ± 45.77 U/L (39) − Creatine kinase isoenzyme CPKIso 290.4 260.83 ± 67.56 U/L (49) − Myoglobin Mb 23.0 0 − 100 μg/L (homo) − Cholinesterase CHE 694.8 766.25 ± 232.49 (42) − Alkaline phosphatase ALP 116.1 117.07 ± 38.60 U/L (40) ↓ γ-yglutamyltranspeptidase GGT 0.2	Albumin/globulin	ALB/GLB	0.68	1.12 ± 0.17 (39)	\
ASpartate aminotransferase/alanine transaminase AST/ALT 1.6 0.91 ± 0.18 (40) ↑ Total bilirubin Direct bilirubin D-BIL 1.2 0.51 ± 0.18 μmol/L (39) ↑ Indirect bilirubin I-BIL 2.3 0.55 ± 0.22 μmol/L (39) ↑ Total bile acids TBA 72.3 75.35 ± 10.18 μmol/L (42) - Alpha-hydroxybutyrate dehydrogenase α-HBDH 833.6 548.30 ± 297.50 U/L (39) - Creatine phosphokinase LDH 951.8 632.59 ± 329.83 U/L (39) - Creatine phosphokinase CPK 175.8 194.96 ± 327.50 U/L (39) - Creatine kinase isoenzyme CPKIso 290.4 260.83 ± 67.56 U/L (39) - Cholinesterase CHE 694.8 766.25 ± 232.49 (42) - Alkaline phosphatase ALP 116.1 117.07 ± 38.60 U/L (40) ↓ α-L-fucosidase AFU 2.6 4.64 ± 1.08 IU/L (40) ↓ Lipase Lip 14.2 0-60 IU/L (homo) Amylase AMY 1.301.5 1.138.26 ± 386.59 U/L (39) - Cystatin c CYS-c 0.21 0.54 ± 0.18 mg/L (41) ↓ Hycersensitive C-reactive protein Adenosine deaminase ADA 8.5 5.47 ± 1.38 U/L (40) ↑ Beta-hydroxybutyric acid β-HB 0.06 0.03-0.3 μmol/L (homo) - 5'nucleotidase 5'-NT 0.6 2.24 ± 1.06 U/L (40) ↓ 5'nucleotidase	Alanine transaminase	ALT	42.0	81.76 ± 19.84 U/L (40)	+
Total bilirubin T-BIL 3.5 1.06 ± 0.29 μmol/L (39) ↑ Direct bilirubin D-BIL 1.2 0.51 ± 0.18 μmol/L (39) ↑ Indirect bilirubin I-BIL 2.3 0.55 ± 0.22 μmol/L (39) ↑ Total bile acids TBA 72.3 75.35 ± 10.18 μmol/L (42) − Alpha-hydroxybutyrate dehydrogenase α-HBDH 833.6 548.30 ± 297.50 U/L (39) − Lactate dehydrogenase LDH 951.8 632.59 ± 329.83 U/L (39) − Creatine phosphokinase CPK 175.8 194.96 ± 45.77 U/L (39) − Creatine kinase isoenzyme CPKIso 290.4 260.83 ± 67.56 U/L (39) − Myoglobin Mb 23.0 0-100 μg/L (homo) − Cholinesterase CHE 694.8 766.25 ± 232.49 (42) − Alkaline phosphatase ALP 116.1 117.07 ± 38.60 U/L (40) − γ-glutamyltranspeptidase GGT 0.2 10.54 ± 6.26 U/L (40) ↓ α-L-fucosidase AFU 2.6 4.64 ± 1.08 IU/L (40)	Aspartate aminotransferase	AST	67.3	71.93 ± 13.34 U/L (40)	-
Direct bilirubin D-BIL 1.2 0.51 ± 0.18 μmol/L (39) ↑ Indirect bilirubin I-BIL 2.3 0.55 ± 0.22 μmol/L (39) ↑ Total bile acids TBA 72.3 75.35 ± 10.18 μmol/L (42) − Alpha-hydroxybutyrate dehydrogenase α-HBDH 833.6 548.30 ± 297.50 U/L (39) − Lactate dehydrogenase LDH 951.8 632.59 ± 329.83 U/L (39) − Creatine phosphokinase CPK 175.8 194.96 ± 45.77 U/L (39) − Creatine kinase isoenzyme CPKIso 290.4 260.83 ± 67.56 U/L (39) − Myoglobin Mb 23.0 0 -100 μg/L (homo) − Cholinesterase CHE 694.8 766.25 ± 232.49 (42) − Alkaline phosphatase ALP 116.1 117.07 ± 38.60 U/L (40) ↓ γ-glutamyltranspeptidase GGT 0.2 10.54 ± 6.26 U/L (40) ↓ α-L-fucosidase AFU 2.6 4.64 ± 1.08 IU/L (40) ↓ Lipase Lip 14.2 0-60 IU/L (homo) − </td <td>Aspartate aminotransferase/alanine transaminase</td> <td>AST/ALT</td> <td>1.6</td> <td>0.91 ± 0.18 (40)</td> <td>↑</td>	Aspartate aminotransferase/alanine transaminase	AST/ALT	1.6	0.91 ± 0.18 (40)	↑
Indirect bilirubin 1-BIL 2.3 0.55 ± 0.22 μmol/L (39) ↑	Total bilirubin	T-BIL	3.5	$1.06 \pm 0.29 \mu$ mol/L (39)	↑
Total bile acids TBA 72.3 75.35 ± 10.18 μmol/L (42) — Alpha-hydroxybutyrate dehydrogenase α-HBDH 833.6 548.30 ± 297.50 U/L (39) — Lactate dehydrogenase LDH 951.8 632.59 ± 329.83 U/L (39) — Creatine phosphokinase CPK 175.8 194.96 ± 45.77 U/L (39) — Creatine kinase isoenzyme CPKIso 290.4 260.83 ± 67.56 U/L (39) — Myoglobin Mb 23.0 0-100 μg/L (homo) — Cholinesterase CHE 694.8 766.25 ± 232.49 (42) — Alkaline phosphatase ALP 116.1 117.07 ± 38.60 U/L (40) — γ-glutamyltranspeptidase GGT 0.2 10.54 ± 6.26 U/L (40) ↓ α-L-fucosidase AFU 2.6 4.64 ± 1.08 IU/L (40) ↓ Lipse Lip 14.2 0-60 IU/L (homo) Amylase AMY 1,301.5 1,138.26 ± 386.59 U/L (39) — Cystatin c CYS-c 0.21 0.54 ± 0.18 mg/L (41) ↓ Hypersensitive C-reactive protein Hs-CRP 0.37 0-3mg/L (homo) — Adenosine deaminase ADA 8.5 5.47 ± 1,38 U/L (40) ↑ Beta-hydroxybutyric acid β-HB 0.06 0.03-0.3 μmol/L (homo) — 5′nucleotidase	Direct bilirubin	D-BIL	1.2	$0.51 \pm 0.18 \mu$ mol/L (39)	↑
Alpha-hydroxybutyrate dehydrogenase α-HBDH 833.6 548.30 ± 297.50 U/L (39) - Lactate dehydrogenase LDH 951.8 632.59 ± 329.83 U/L (39) - Creatine phosphokinase CPK 175.8 194.96 ± 45.77 U/L (39) - Creatine kinase isoenzyme CPKIso 290.4 260.83 ± 67.56 U/L (39) - Myoglobin Mb 23.0 0-100 μg/L (homo) - Cholinesterase CHE 694.8 766.25 ± 232.49 (42) - Alkaline phosphatase ALP 116.1 117.07 ± 38.60 U/L (40) - γ-glutamyltranspeptidase GGT 0.2 10.54 ± 6.26 U/L (40) ↓ α-L-fucosidase AFU 2.6 4.64 ± 1.08 IU/L (40) ↓ Lipase Lip 14.2 0-60 IU/L (homo) - Amylase AMY 1,301.5 1,138.26 ± 386.59 U/L (39) - Cystatin c CYS-c 0.21 0.54 ± 0.18 mg/L (41) ↓ Hypersensitive C-reactive protein Hs-CRP 0.37 0-3mg/L (homo) - Adenosine deaminase ADA 8.5 5.47 ± 1.38 U/L (40	Indirect bilirubin	I-BIL	2.3	$0.55 \pm 0.22 \mu$ mol/L (39)	↑
Lactate dehydrogenase LDH 951.8 632.59 ± 329.83 U/L (39) - Creatine phosphokinase CPK 175.8 194.96 ± 45.77 U/L (39) - Creatine kinase isoenzyme CPKIso 290.4 260.83 ± 67.56 U/L (39) - Myoglobin Mb 23.0 0 −100 μg/L (homo) - Cholinesterase CHE 694.8 766.25 ± 232.49 (42) - Alkaline phosphatase ALP 116.1 117.07 ± 38.60 U/L (40) - γ-glutamyltranspeptidase GGT 0.2 10.54 ± 6.26 U/L (40) ↓ α-L-fucosidase AFU 2.6 4.64 ± 1.08 IU/L (40) ↓ Lipase Lip 14.2 0 −60 IU/L (homo) - Amylase AMY 1,301.5 1,138.26 ± 386.59 U/L (39) - Cystatin c CYS-c 0.21 0.54 ± 0.18 mg/L (41) ↓ Hypersensitive C-reactive protein Hs-CRP 0.37 0-3mg/L (homo) - Adenosine deaminase ADA 8.5 5.47 ± 1.38 U/L (40) ↑	Total bile acids	TBA	72.3	$75.35 \pm 10.18 \mu$ mol/L (42)	-
Creatine phosphokinase CPK 175.8 194.96 ± 45.77 U/L (39) - Creatine kinase isoenzyme CPKIso 290.4 260.83 ± 67.56 U/L (39) - Myoglobin Mb 23.0 0-100 μg/L (homo) - Che 694.8 766.25 ± 232.49 (42) - Alkaline phosphatase ALP 116.1 117.07 ± 38.60 U/L (40) - γ-glutamyltranspeptidase GGT 0.2 10.54 ± 6.26 U/L (40) ↓ α-L-fucosidase AFU 2.6 4.64 ± 1.08 IU/L (40) ↓ Lipase Lip 14.2 0-60 IU/L (homo) _ Amylase AMY 1,301.5 1,138.26 ± 386.59 U/L (39) - Cystatin c CYS-c 0.21 0.54 ± 0.18 mg/L (41) ↓ Hypersensitive C-reactive protein Hs-CRP 0.37 0-3mg/L (homo) - Adenosine deaminase ADA 8.5 5.47 ± 1.38 U/L (40) ↑ Beta-hydroxybutyric acid β-HB 0.06 0.03-0.3 μmol/L (homo) - 5'-NT 0.6	Alpha-hydroxybutyrate dehydrogenase	α-HBDH	833.6	548.30 ± 297.50 U/L (39)	-
Creatine kinase isoenzyme CPKIso 290.4 260.83 ± 67.56 U/L (39) − Myoglobin Mb 23.0 0−100 μg/L (homo) − Cholinesterase CHE 694.8 766.25 ± 232.49 (42) − Alkaline phosphatase ALP 116.1 117.07 ± 38.60 U/L (40) − γ-glutamyltranspeptidase GGT 0.2 10.54 ± 6.26 U/L (40) ↓ α-L-fucosidase AFU 2.6 4.64 ± 1.08 IU/L (40) ↓ Lipase Lip 14.2 0−60 IU/L (homo) → Amylase AMY 1,301.5 1,138.26 ± 386.59 U/L (39) − Cystatin c CYS-c 0.21 0.54 ± 0.18 mg/L (41) ↓ Hypersensitive C-reactive protein Hs-CRP 0.37 0-3mg/L (homo) − Adenosine deaminase ADA 8.5 5.47 ± 1.38 U/L (40) ↑ Beta-hydroxybutyric acid β-HB 0.06 0.03-0.3 μmol/L (homo) − 5'nucleotidase 5'-NT 0.6 2.24 ± 1.06 U/L (40) ↓	Lactate dehydrogenase	LDH	951.8	632.59 ± 329.83 U/L (39)	-
Myoglobin Mb 23.0 0-100 μg/L (homo) - Cholinesterase CHE 694.8 766.25 ± 232.49 (42) - Alkaline phosphatase ALP 116.1 117.07 ± 38.60 U/L (40) - γ-glutamyltranspeptidase GGT 0.2 10.54 ± 6.26 U/L (40) ↓ α-L-fucosidase AFU 2.6 4.64 ± 1.08 IU/L (40) ↓ Lipase Lip 14.2 0-60 IU/L (homo) _ Amylase AMY 1,301.5 1,138.26 ± 386.59 U/L (39) - Cystatin c CYS-c 0.21 0.54 ± 0.18 mg/L (41) ↓ Hypersensitive C-reactive protein Hs-CRP 0.37 0-3mg/L (homo) - Adenosine deaminase ADA 8.5 5.47 ± 1.38 U/L (40) ↑ Beta-hydroxybutyric acid β-HB 0.06 0.03-0.3 μmol/L (homo) - 5'nucleotidase 5'-NT 0.6 2.24 ± 1.06 U/L (40) ↓	Creatine phosphokinase	СРК	175.8	194.96 ± 45.77 U/L (39)	_
Cholinesterase CHE 694.8 766.25 ± 232.49 (42) - Alkaline phosphatase ALP 116.1 117.07 ± 38.60 U/L (40) - γ-glutamyltranspeptidase GGT 0.2 10.54 ± 6.26 U/L (40) ↓ α-L-fucosidase AFU 2.6 4.64 ± 1.08 IU/L (40) ↓ Lipase Lip 14.2 0-60 IU/L (homo) _ Amylase AMY 1,301.5 1,138.26 ± 386.59 U/L (39) - Cystatin c CYS-c 0.21 0.54 ± 0.18 mg/L (41) ↓ Hypersensitive C-reactive protein Hs-CRP 0.37 0-3mg/L (homo) - Adenosine deaminase ADA 8.5 5.47 ± 1.38 U/L (40) ↑ Beta-hydroxybutyric acid β-HB 0.06 0.03-0.3 μ mol/L (homo) - 5'nucleotidase 5'-NT 0.6 2.24 ± 1.06 U/L (40) ↓	Creatine kinase isoenzyme	CPKIso	290.4	260.83 ± 67.56 U/L (39)	-
Alkaline phosphatase	Myoglobin	Mb	23.0	0–100 μg/L (homo)	-
γ-glutamyltranspeptidase GGT 0.2 10.54 ± 6.26 U/L (40) ↓ α-L-fucosidase AFU 2.6 4.64 ± 1.08 IU/L (40) ↓ Lipase Lip 14.2 $0-60$ IU/L (homo) Amylase AMY $1,301.5$ $1,138.26 \pm 386.59$ U/L (39) - Cystatin c CYS-c 0.21 0.54 ± 0.18 mg/L (41) ↓ Hypersensitive C-reactive protein Hs-CRP 0.37 $0-3$ mg/L (homo) - Adenosine deaminase ADA 8.5 5.47 ± 1.38 U/L (40) ↑ Beta-hydroxybutyric acid β -HB 0.06 $0.03-0.3$ µmol/L (homo) - 5'nucleotidase $5'$ -NT 0.6 2.24 ± 1.06 U/L (40) ↓	Cholinesterase	CHE	694.8	766.25 ± 232.49 (42)	-
α-L-fucosidase AFU 2.6 $4.64 \pm 1.08 \text{ IU/L}$ (40) ↓ Lipase Lip 14.2 $0-60 \text{ IU/L}$ (homo)	Alkaline phosphatase	ALP	116.1	117.07 ± 38.60 U/L (40)	_
Lip 14.2 0-60 IU/L (homo) Amylase AMY 1,301.5 1,138.26 ± 386.59 U/L (39) - Cystatin c CYS-c 0.21 0.54 ± 0.18 mg/L (41) ↓ Hypersensitive C-reactive protein Hs-CRP 0.37 0-3mg/L (homo) - Adenosine deaminase ADA 8.5 5.47 ± 1.38 U/L (40) ↑ Beta-hydroxybutyric acid β -HB 0.06 0.03-0.3 μ mol/L (homo) - 5'nucleotidase $5'$ -NT 0.6 2.24 ± 1.06 U/L (40) ↓	γ-glutamyltranspeptidase	GGT	0.2	10.54 ± 6.26 U/L (40)	↓
Amylase AMY 1,301.5 1,138.26 ± 386.59 U/L (39) - Cystatin c CYS-c 0.21 0.54 ± 0.18 mg/L (41) ↓ Hypersensitive C-reactive protein Hs-CRP 0.37 0-3mg/L (homo) - Adenosine deaminase ADA 8.5 5.47 ± 1.38 U/L (40) ↑ Beta-hydroxybutyric acid β -HB 0.06 0.03-0.3 μ mol/L (homo) - 5'nucleotidase $5'$ -NT 0.6 2.24 ± 1.06 U/L (40) ↓	α-L-fucosidase	AFU	2.6	4.64 ± 1.08 IU/L (40)	↓
Cystatin c CYS-c 0.21 0.54 ± 0.18 mg/L (41) ↓ Hypersensitive C-reactive protein Hs-CRP 0.37 0-3mg/L (homo) - Adenosine deaminase ADA 8.5 5.47 ± 1.38 U/L (40) ↑ Beta-hydroxybutyric acid β-HB 0.06 $0.03-0.3$ μmol/L (homo) - 5'nucleotidase 5'-NT 0.6 2.24 ± 1.06 U/L (40) ↓	Lipase	Lip	14.2	0-60 IU/L (homo)	
Hypersensitive C-reactive protein Hs-CRP 0.37 0-3mg/L (homo) - Adenosine deaminase ADA 8.5 5.47 ± 1.38 U/L (40) ↑ Beta-hydroxybutyric acid β -HB 0.06 $0.03-0.3 \mu$ mol/L (homo) - 5'nucleotidase $5'$ -NT 0.6 2.24 ± 1.06 U/L (40) ↓	Amylase	AMY	1,301.5	1,138.26 ± 386.59 U/L (39)	-
Adenosine deaminase ADA 8.5 5.47 ± 1.38 U/L (40) ↑ Beta-hydroxybutyric acid β-HB 0.06 $0.03-0.3$ μmol/L (homo) - 5'nucleotidase $5'$ -NT 0.6 2.24 ± 1.06 U/L (40) ↓	Cystatin c	CYS-c	0.21	$0.54 \pm 0.18 \text{ mg/L (41)}$	↓
Beta-hydroxybutyric acid β-HB 0.06 0.03-0.3 μ mol/L (homo) - 5'nucleotidase 5'-NT 0.6 2.24 ± 1.06 U/L (40) ↓	Hypersensitive C-reactive protein	Hs-CRP	0.37	0-3mg/L (homo)	-
5'nucleotidase 5'-NT 0.6 2.24 ± 1.06 U/L (40)	Adenosine deaminase	ADA	8.5	5.47 ± 1.38 U/L (40)	↑
	Beta-hydroxybutyric acid	β-НВ	0.06	0.03-0.3 μmol/L (homo)	-
Ischaemic modified albumin IMA 61.0 > 64.7 U/ml (homo) \downarrow	5'nucleotidase	5'-NT	0.6	2.24 ± 1.06 U/L (40)	\
	Ischaemic modified albumin	IMA	61.0	> 64.7 U/ml (homo)	↓

The routine blood test of this giant panda was carried out on Mindray BC5500 (Mindray Medical International Co., LTD, Shenzhen, China) and the blood biochemistry test of this giant panda was carried out on Mindray BS-600M (Mindray Medical International Co., LTD, Shenzhen, China). The reference range of each indicator is detailed in the reference. # =count.

long-term feeding and management until its death, we did not find any abnormalities in its two hind limbs.

3 Discussion

Osteomyelitis, characterized by inflammation of the periosteum, sclerotin, and bone marrow, and it is caused by purulent bacteria (26). Based on the disease progression, it can be categorized into acute and chronic forms. Acute osteomyelitis progresses rapidly, often accompanied hyperpyrexia and toxemia. Typical clinical signs and manifestations of infection include erythema, swelling, warmth, and pain. Blood examinations usually reveal elevated leukocyte and neutrophil counts. Notably, due to the evolving virulence of pathogenic bacteria and enhanced host resistance, subacute or chronic osteomyelitis frequently occurs, presenting with insidious symptoms such as joint pain in the

affected bone or adjacent joints. This poses significant challenges to clinical diagnosis (1, 13).

In general, acute osteomyelitis is associated with elevated leukocytes, neutrophils, and C-reactive protein (CRP) (27). However, in this case, laboratory clinical examination showed no increase in leukocytes, neutrophils, or CRP, strongly suggesting that the condition was not acute. An increase in TC and TG indicates hyperlipidemia and requires dietary adjustments. However, these indicators are likely not associated with the onset of osteomyelitis.

CT provides high density resolution, enabling clear detection of bone damage, particularly cortical bone destruction Early subperiosteal abscess formation can be identified by quantitative analysis of lesion attenuation values (28). However, conventional CT, as used in the present study, has limited sensitivity for detecting early marrow involvement in osteomyelitis. In its early stages, osteomyelitis may lack characteristic findings such as lysis, soft tissues changes, or clear inflammatory infiltration, making accurate localization and assessment of lesion extent challenging

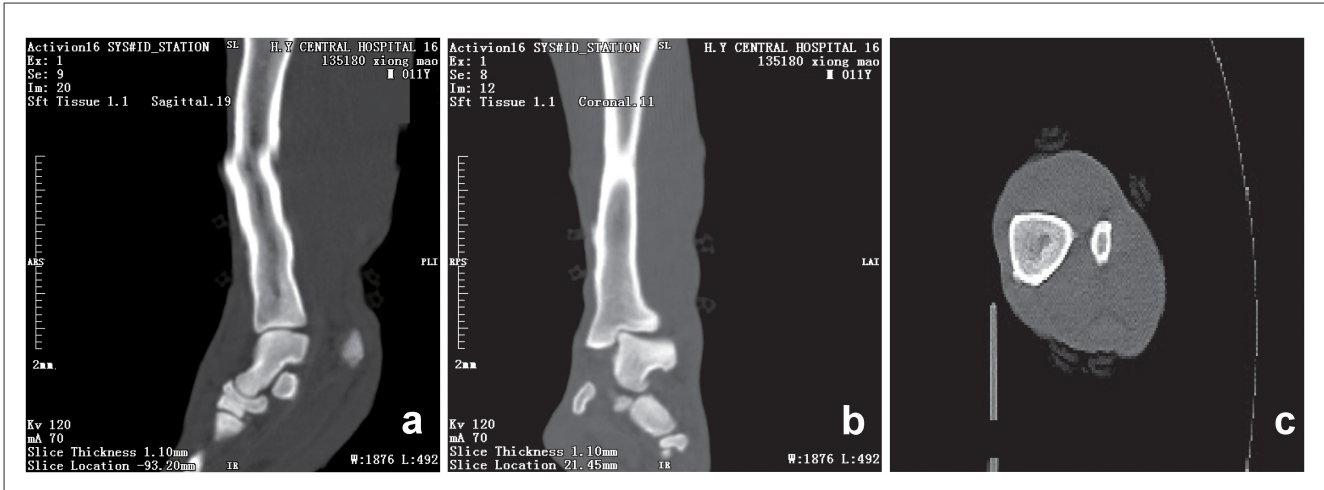


FIGURE 2

CT scans of the hind limb of the giant panda. Sagittal (a), coronal (b) and transverse (c) computed tomography (CT) scan of the left hind limb showing smooth, well-defined articular margins. The tarsal bones are correctly aligned, and corticomedullary definition is normal. The distal tibial articular surface shows a normal inclination angle. No fractures are observed. The osseous structures of the included joints are intact with no adjacent significant soft tissue swelling. A slight step artifact is present in the mid and distal diaphysis of the tibia. Scan parameters: tube voltage = 120 kV; tube current = 70 mA; slice thickness = 1.10 mm; window width (WW) = 1,876 HU; window level (WL) = 492 HU; reconstructed using a soft tissue 1.1 sequence.



FIGURE

Magnetic resonance image of left hind limb of giant panda. (a) T1W sequence of sagittal plane. Sequence Parameters: repeat time (TR) of 1,700 ms, echo time (TE) 15 ms, slice thickness of 3.8 mm, window width (W) of 6,438 HU, and window level (L) of 3,192 HU. Bony structures (distal tibia, talus, calcaneus) show clear margins with homogeneous bone marrow signal (isointense to muscle on T1W). Articular cartilage appears smooth with isointense signal; No definite bony cortex disruption or abnormal signal involvement of bones. (b) T2W sequence of transverse plane. Sequence Parameters: repeat time (TR) of 4,294 ms, echo time (TE) 105 ms, slice thickness of 5 mm, window width (W) of 7,031 HU, and window level (L) of 2,678 HU. Patchy hyperintensities (long T2 signal, suggestive of edema/inflammation) are noted in soft tissues around the distal tibia (internuscular space); Focal hyperintensities are observed in soft tissues posterior to the calcaneus (around the Achilles tendon), with clear demarcation from the tendon.

(29). Notably, dual-energy CT—an advanced modality capable of detecting bone edema—was not available for this study. Although quantitative analysis of CT attenuation values may improve detection of early lesions, this was not performed in the present cases. Consistent with the limitations of conventional CT in identifying subtle early changes, CT findings were normal,

prompting additional MRI examination to clarify the condition. MRI, provides higher soft tissue resolution and contrast, excelling in detecting early marrow changes, making it a preferred for early diagnosis of osteomyelitis (30). The MRI results of the giant panda's lower limb showed isointense signals on T1WI, indicating normal bone morphology, which was consistent with

the CT findings. However, the high signal on T2WI indicated the presence of a lesions. Given that this giant panda had no recent history of trauma, and its MRI scans revealed no trauma-specific imaging features—such as fracture lines, acute bone marrow contusions with diffuse hemorrhagic signals, or signs of soft tissue laceration—these findings effectively ruled out traumatic abnormalities in bone marrow signals. Similarly, no masses were noted on imaging, suggesting the absence of neoplastic lesions. Thus, the combined use of CT and MRI in this giant panda case highlights their complementary roles in diagnosing bone and soft tissue abnormalities. While CT effectively rules out gross bony lesions, MRI's superior sensitivity to early marrow changes and soft tissue pathology enables the detection of subtle lesions that may indicate early-stage osteomyelitis.

Upon diagnosing osteomyelitis, veterinarians opted for conservative oral antibiotic treatment to prevent disease progression in this geriatric giant panda, as surgical and intravenous therapies posed high risks (e.g., anesthesia complications, management challenges).

Rifampicin, a broad-spectrum antibiotic, inhibits bacterial RNA polymerase, acting against pathogens such as Staphylococcus aureus and Mycobacterium tuberculosis (31). Chitosan, a natural polysaccharide, exhibits anti-inflammatory, tissue repairpromoting, immunomodulatory, and moderate antibacterial properties (32, 33). The combined application of rifampicin and chitosan has been reported to be effective in the treatment of osteomyelitis, especially in cases of bacterial L- form infections or hypertrophic osteoarthropathy resulting from inappropriate antibiotic selection, with a low incidence of adverse reaction (34). Moreover, it has shown unique therapeutic effects in subacute and chronic osteomyelitis of human (35). The pharmacological mechanism of their combined is based on a triple approach "antibacterial-anti-inflammatory-repair-promoting," enhances bacterial clearance, reduce inflammatory damage, and promotes bone tissue regeneration. In veterinary medicine, the use of this combination remains primarily experimental, as there is currently no established standard practice for its application in wildlife. Supporting evidence in veterinary species is limited but includes extrapolation from human clinical data and preliminary studies in domestic mammals (e.g., rabbits, horses) demonstrating comparable antibacterial and tissue-repair effects (36-38). For this case, rifampicin and chitosan were administered separately (not as compound preparation). The administration regimen for giant pandas was based on the animal's weight $(\sim 120 \,\mathrm{kg})$ and administered by referring to the therapeutic dose in humans or in human patients. In addition, based on the clinical experience of the veterinary team in treating captive giant pandas with antibiotics, the dosage was fine-tuned to balance efficacy and safety.

The combination therapy yielded positive outcomes, with the panda's lameness resolving and no recurrence observed after discontinuation. However, this case was constrained by significant limitations: bacterial culture was not performed due to challenges in obtaining adequate samples (e.g., avoiding iatrogenic injury to the giant panda during sample collection from deep bone lesions), leaving the causative pathogen unidentified. This hindered precise antibiotic selection, manifested as the initial ineffectiveness of antibiotics and reduced the study's scientific rigor.

To address these limitations in future cases, targeted improvements in diagnostic and therapeutic strategies are of paramount importance. For diagnostic advancements, priority should be given to optimizing sample collection protocols: minimally invasive techniques (e.g., ultrasound-guided needle aspiration of abscesses or bone marrow biopsies) should be employed to obtain lesion-derived samples while minimizing stress to the animal. Furthermore, integrating advanced molecular diagnostic tools-such as 16S rRNA gene sequencing or metagenomic analysis-can facilitate the identification of fastidious pathogens that are difficult to culture. Simultaneous implementation of aerobic and anaerobic bacterial cultures, combined with antimicrobial susceptibility testing (AST), will further enable precise pathogen identification and guide evidencebased antibiotic selection, thereby reducing reliance on empirical therapy. In terms of therapeutic refinement, future protocols should emphasize individualized dosing strategies tailored to the unique physiological characteristics of giant pandas. This includes leveraging pharmacokinetic studies in captive giant pandas or phylogenetically related species (e.g., bears) to establish speciesspecific drug metabolism parameters, ensuring optimal dosing of rifampicin, chitosan, or alternative agents. Collectively, these measures will address the current gaps in pathogen identification and therapeutic precision, strengthening the scientific basis for the management of osteomyelitis in giant pandas and other species.

Although this research report has limitations, it represents the first reported case of osteomyelitis diagnosis and treatment in giant pandas. It is hoped that this report can serve as a valuable reference for future clinical diagnosis, treatment, breeding, and management of giant pandas.

Data availability statement

The original contributions presented in the study are included in the article/supplementary material, further inquiries can be directed to the corresponding author.

Ethics statement

The animal study was approved by Experimental Animal Ethics Review Committee of China Conservation and Research Center of the Giant Pandas. The study was conducted in accordance with the local legislation and institutional requirements. Written informed consent was obtained from the participants for the publication of this case report.

Author contributions

CW: Writing – review & editing, Conceptualization. HY: Data curation, Writing – review & editing. KW: Resources, Writing – review & editing. LD: Writing – review & editing, Data curation. ChL: Software, Writing – original draft. RW: Supervision, Writing – review & editing. CaL: Writing – review & editing, Investigation. YZ: Writing – original draft, Investigation. MW: Project administration, Writing – review & editing. ZH: Project

administration, Writing – review & editing. YC: Writing – review & editing, Data curation. XC: Project administration, Writing – review & editing. DL: Funding acquisition, Writing – review & editing, Supervision.

Funding

The author(s) declare that financial support was received for the research and/or publication of this article. The study was supported by the key project of the National Forestry and Grassland Administration of China under Grant [number CGF2024001].

Conflict of interest

The authors declare that the research was conducted in the absence of any commercial or financial relationships that could be construed as a potential conflict of interest.

References

- 1. Lew DP, Waldvogel FA. Osteomyelitis. *Lancet.* (2004) 364:369–79. doi:10.1016/S0140-6736(04)16727-5
- 2. Bariteau JT, Waryasz GR, McDonnell M, Fischer SA, Hayda RA, Born CT. Fungal osteomyelitis and septic arthritis. *J Am Acad Orthop Surg.* (2014) 22:390–401. doi: 10.5435/JAAOS-22-06-390
- 3. Sommer T, Karsy M, Driscoll MJ, Jensen RL. Varicella-zoster virus infection and osteomyelitis of the skull. *World Neurosurg.* (2018) 115:297–300. doi: 10.1016/j.wneu.2018.04.194
- 4. Hogan A, Heppert VG, Suda AJ. Osteomyelitis. Arch Orthop Trauma Surg. (2013) 133:1183–96. doi: 10.1007/s00402-013-1785-7
- 5. Johnson KA. Osteomyelitis in dogs and cats. J Am Vet Med Assoc. (1994) 204:1882–7. doi: 10.2460/javma.1994.204.12.1882
- 6. Whitman RE, Wilson NA, Heseltine JC. Prototheca osteomyelitis in a dog. $Can\ Vet\ J.\ (2025)\ 66:46-50.$
- 7. Hui J, Ryan KA, Rademacher N, Neupane P. Breitschwerdt EB. Osteomyelitis associated with *Bartonella henselae* infection in a young cat. *JFMS Open Rep.* (2022) 8:20551169221124910. doi: 10.1177/20551169221124910
- 8. Schoiswohl J, Degasperi B, Schieder K, Ertelt K, Kofler J. Limb amputation in 2 small ruminants. *Tierarztl Prax Ausg G Grosstiere Nutztiere*. (2020) 48:191–7. doi: 10.1055/a-1162-0247
- 9. Ciammaichella L, Cola V, Foglia A, Zanardi S, Chalfon C, Tassani C, et al. Haematogenous polyostotic osteomyelitis caused by *Serratia marcescens* in a cat. *Top Companion Anim Med.* (2024) 63:100924. doi: 10.1016/j.tcam.2024.100924
- 10. Bury DC, Rogers TS, Dickman MM. Osteomyelitis: diagnosis and treatment. Am Fam Physician. (2021) 104:395–402.
- 11. Ramachandran S, Zhao Y, Ferguson PJ. Update on treatment responses and outcome measure development in chronic nonbacterial osteomyelitis. *Curr Opin Rheumatol.* (2023) 35:255–64. doi: 10.1097/BOR.0000000000000954
- 12. Alhinai Z, Elahi M, Park S, Foo B, Lee B, Chapin K, et al. Prediction of adverse outcomes in pediatric acute hematogenous osteomyelitis. *Clin Infect Dis.* (2020) 71:e454–64. doi: 10.1093/cid/ciaa211
- 13. Hatzenbuehler J, Pulling TJ. Diagnosis and management of osteomyelitis. *Am Fam Physician*. (2011) 84:1027–33.
- 14. Holt JG, Laughlin JS, Moroney JP. The extension of the concept of tissue-air ratios (TAR) to high-energy x-ray beams. *Radiology*. (1970) 96:437–46. doi: 10.1148/96.2.437
- 15. Kanis JA. Assessment of fracture risk and its application to screening for postmenopausal osteoporosis: synopsis of a WHO report. WHO study group. *Osteoporos Int.* (1994) 4:368–81. doi: 10.1007/BF01622200
- 16. Birnbacher L, Braig EM, Pfeiffer D, Pfeiffer F, Herzen J. Quantitative X-ray phase contrast computed tomography with grating interferometry: biomedical applications

Generative AI statement

The author(s) declare that no Gen AI was used in the creation of this manuscript.

Any alternative text (alt text) provided alongside figures in this article has been generated by Frontiers with the support of artificial intelligence and reasonable efforts have been made to ensure accuracy, including review by the authors wherever possible. If you identify any issues, please contact us.

Publisher's note

All claims expressed in this article are solely those of the authors and do not necessarily represent those of their affiliated organizations, or those of the publisher, the editors and the reviewers. Any product that may be evaluated in this article, or claim that may be made by its manufacturer, is not guaranteed or endorsed by the publisher.

- of quantitative X-ray grating-based phase contrast computed tomography. Eur J Nucl Med Mol Imaging. (2021) 48:4171–88. doi: 10.1007/s00259-021-05259-6
- 17. Ginat DT, Gupta R. Advances in computed tomography imaging technology. *Annu Rev Biomed Eng.* (2014) 16:431–53. doi: 10.1146/annurev-bioeng-121813-113601
- 18. Aihuai D, Chunyu G. Clinical application research of anesthetics in wild animals (in Chinese). *Chin Abstr Anim Husb Vet Med.* (2016) 32:232.
- 19. Hagag U, Nahas AE, Almohamad ZA, Brehm W, Gerlach K. 3T Magnetic resonance imaging and computed tomography of the bovine carpus. *BMC Vet Res.* (2022) 18:236. doi: 10.1186/s12917-022-03346-w
- 20. Garrett KS. When radiography and ultrasonography are not enough: the use of computed tomography and magnetic resonance imaging for equine lameness cases. *J Am Vet Med Assoc.* (2022) 260:1113–23. doi: 10.2460/javma.22.03.0136
- 21. Chandnani VP, Beltran J, Morris CS, Khalil SN, Mueller CF, Burk JM, et al. Acute experimental osteomyelitis and abscesses: detection with MR imaging versus CT. *Radiology*. (1990) 174:233–6. doi: 10.1148/radiology.174.1.2294554
- 22. Calivà F, Namiri NK, Dubreuil M, Pedoia V, Ozhinsky E, Majumdar S. Studying osteoarthritis with artificial intelligence applied to magnetic resonance imaging. *Nat Rev Rheumatol.* (2022) 18:112–21. doi: 10.1038/s41584-021-00719-7
- 23. Palestro CJ. Radionuclide imaging of musculoskeletal infection: a review. *J Nucl Med.* (2016) 57:1406–12. doi: 10.2967/jnumed.115.157297
- 24. Govaert GA, IJpma FF, McNally M, McNally E, Reininga IH, Glaudemans AW. Accuracy of diagnostic imaging modalities for peripheral post-traumatic osteomyelitis a systematic review of the recent literature. *Eur J Nucl Med Mol Imaging.* (2017) 44:1393–407. doi: 10.1007/s00259-017-3683-7
- 25. Brocal J, Del Río FR, Feliu-Pascual AL. Diagnosis and management of lumbar *Aspergillus* spp. discospondylitis using intraoperative cytology and external stabilization in a dog with disseminated infection. *Open Vet J.* (2019) 9:185–9. doi: 10.4314/ovj.v9i3.1
- 26. Momodu II, Savaliya V. Osteomyelitis. In: StatPearls. StatPearls Publishing LLC (2024).
- 27. Rodríguez Lorenzo P, Fernández Martínez B, Pérez Alba M, Ramírez Jaén C, Meana Morís AR, Pérez Méndez C. Primary sternal osteomyelitis. *Arch Argent Pediatr.* (2023) 121:e202201449. doi: 10.5546/aap.2022-01449.eng
- 28. Lee SJ, Won KS, Choi HJ, Choi YY. Early-phase SPECT/CT for diagnosing osteomyelitis: a retrospective pilot study. *Korean J Radiol.* (2021) 22:604–11. doi: 10.3348/kjr.2019.0746
- 29. Lee YJ, Sadigh S, Mankad K, Kapse N, Rajeswaran G. The imaging of osteomyelitis. *Quant Imaging Med Surg.* (2016) 6:184–98. doi:10.21037/qims.2016.04.01
- 30. Dobaria DG, Cohen HL. Osteomyelitis imaging. In: StatPearls. StatPearls Publishing LLC (2025).

- 31. Zelmer AR, Yang D, Gunn NJ, Solomon LB, Nelson R, Kidd SP, et al. Osteomyelitis-relevant antibiotics at clinical concentrations show limited effectivity against acute and chronic intracellular *S. aureus* infections in osteocytes. *Antimicrob Agents Chemother*. (2024) 68:e0080824. doi: 10.1128/aac.00808-24
- 32. Tucker LJ, Grant CS, Gautreaux MA, Amarasekara DL, Fitzkee NC, Janorkar AV, et al. Physicochemical and antimicrobial properties of thermosensitive chitosan hydrogel loaded with fosfomycin. *Mar Drugs*. (2021) 19:144. doi: 10.3390/md19030144
- 33. Zegre M, Barros J, David AB, Fialho L, Ferraz MP, Monteiro FJ, et al. Dual-loaded chitosan-based nanoparticles: a novel approach for treating polymicrobial osteomyelitis. *Int J Pharm.* (2025) 674:125480. doi: 10.1016/j.ijpharm.2025.125480
- 34. Lefebvre M, Jacqueline C, Amador G, Le Mabecque V, Miegeville A, Potel G, et al. Efficacy of daptomycin combined with rifampicin for the treatment of experimental meticillin-resistant *Staphylococcus aureus* (MRSA) acute osteomyelitis. *Int J Antimicrob Agents*. (2010) 36:542–4. doi: 10.1016/j.ijantimicag.2010.07.008
- 35. Wang B. The effect of rifampicin and chitosan on chronic osteomyelitis. *Chin J Orthop Traumatol.* (2000) 13:651–52.
- 36. Clark-Price SC, Rush BR, Gaughan EM, Cox JH. Osteomyelitis of the pelvis caused by Rhodococcus equi in a two-year-old horse. *J Am Vet Med Assoc.* (2003) 222:969–72, 952–3. doi: 10.2460/javma.2003.222.969

- 37. Rissing JP. Animal models of osteomyelitis. Knowledge, hypothesis, and speculation. *Infect Dis Clin North Am.* (1990) 4:377–90. doi: 10.1016/S0891-5520(20)30352-4
- 38. Qian L, Zhaohui Z, Yaping X, Zhentian L, Zhentao L, Qiqi W, et al. Blood T cell diversity associated with the prognosis of advanced non-small cell lung carcinoma treated with first-line pemetrexed based chemotherapy. *Thorac Cancer*. (2021) 12:997–1005. doi: 10.1111/1759-7714.13771
- 39. Li L, Jingchao L, Li L, Wenjun H, Lihui L, Xin C, et al. Hematologic and biochemical reference of captive giant pandas based on non-stress sampling methods. *Chin J Wildlife.* (2017) 38:7.
- 40. Linhua D, Yan C, Rongping W, Chengdong W, Shan H, Ming W, et al. Seasonal changes of physiological and blood indices of captive giant panda. *Acta Theriologica Sinica*. (2020) 40:398–406.
- 41. Changmeng Y, Yao Y, Denghu W, Jun Z, Bingbing Y. Determination and analysis of blood physiological and biochemical indexes of giant pandas in Chongqing zoo. *Chin J Wildlife*. (2019) 40:33–42.
- 42. Min Z, Yu Z, Zhu M, Yanxi C, Lei J, Jing W, et al. Determination and analysis of trace elements, clinical indicators, and physiological-biochemical blood indices of captive giant panda. *Chin J Wildlife*. (2021) 42:44–55.